Lattice Boltzmann spray-like fluids

G. Falcucci[1], S. Chibbaro[2,3] S. Succi[2], X. Shan[4] and H. Chen[4]

[1] *Dept. of Mechanical and Industrial Engineering, University of "Roma Tre", Via della Vasca Navale 79, Rome, Italy*
[2] *Istituto Applicazioni Calcolo "Mauro Picone", CNR, V.le del Policlinico 137, Rome, Italy*
[3] *Dept. of Mechanical Engineering, University of "Tor Vergata", Viale Politecnico, Rome, Italy*
[4] *EXA Corporation, 450 Bedford Street, Lexington, Massachussetts 02173*

PACS 47.11.-j – First pacs description
PACS 47.55.Ca – Second pacs description
PACS 47.55.dk – Third pacs description

Abstract. - The effects of the competition between short-range attraction and mid-range repulsion in lattice Boltzmann models of single-component non-ideal fluids is investigated. It is shown that the presence of repulsive interactions gives rise to long-lived metastable states in the form of multi-droplet spray-like density configurations, whose size can be adjusted by fine-tuning the strength of the repulsive versus attractive coupling. This opens up the possibility of using single-component lattice kinetic models to study a new class of complex flow applications, involving atomization, spray formation, micro-emulsions and possibly, glassy-like phenomena as well.

The dynamics of multi-phase flows with complex translational/rotational order is a rich branch of modern science, lying at the interface between fluid dynamics and condensed matter, with many applications in physics, chemistry, engineering and life-sciences [1, 2]. Although phase-transitions from isotropic, homogeneous fluids to anisotropic/ordered ones can be traced to a large variety of underlying microscopic conditions, a common feature of many microscopic scenarios is the competition between short-range attraction and mid/long-range repulsion [3]. Short-range attraction typically drives phase-separation through dynamical instabilities towards density perturbations in the fluid, whereas mid/long-range repulsion frustrates this tendency, thus giving rise to a variety of complex symmetry-breaking structures within the flow. The analytical study of these phenomena is obviously a difficult one, mainly due to the need of accounting for the simultaneous interaction of many disparate scales. Consequently, the investigation of multiphase flows, both classical and quantum, is in a constant need of flexible and efficient computational methods. The task of simulating the behaviour of multiphase flows is however a very challenging one, due to the emergence of moving interfaces with complex topology [7]. In the last decade, a new class of mesoscopic methods, based on minimal lattice formulations of Boltzmann's kinetic equation, have captured significant interest as an efficient and flexible alternative to continuum methods based on the discretization of the Navier-Stokes equations for non-ideal fluids [8–12]. To date, a very popular mesoscopic approach is the so-called pseudo-potential-Lattice-Boltzmann (LB) method, developed over a decade ago by Shan and Chen (SC) [13]. This method has gained increasing popularity on account of its simplicity and computational efficiency. In the SC method, potential energy interactions are represented through a density-dependent mean-field pseudo-potential, $\psi(\rho)$, and phase separation is achieved by imposing a short-range attraction between the light and dense phases. To date, the SC pseudo-potential has only been used in its original version, where only nearest-neighbour attractive interactions are included. This implies that, in the absence of external constraints, the time-asymptotic state of the phase-separated fluid corresponds to a single droplet configuration. Very recently, however, it has been pointed out that the inclusion of mid-ranged potentials, extending beyond nearest-neighbour interactions, may open up new perspectives and applications of the SC model. In particular, it has been conjectured that mid-range repulsion should be able to interrupt the phase-separation induced by short-range attraction, thereby providing a physical mechanism promoting the onset of metastable states in the form of long-lived droplets of different size [14]. This idea has been pursued before in many endeavors [4–6], including lattice-gas cellular automata [15]. However, to the best of

our knowledge, this is the first time that the idea is applied to the Lattice-Boltzmann framework. In this Letter, we provide numerical evidence that a mesoscopic lattice Boltzmann model with mid-range repulsion is indeed capable of sustaining long-lived metastable states in the form of multi-droplet spray-like configurations, whose size and number can be controlled by tuning the strength of repulsive interactions. This opens up the possibility of deploying the computational power of lattice kinetic methods to study a variety of very complex fluids flows such sprays, emulsions and glassy-like materials, which are hard to simulate with the standard Shan-Chen model. The kinetic lattice Boltzmann equation writes as follows [16, 17]:

$$\begin{aligned} f_i(\vec{r}+\vec{c}_i\Delta t, t+\Delta t) &- f_i(\vec{r},t) = \\ -\frac{1}{\tau}[f_i(\vec{r},t) &- f_i^{(eq)}(\vec{r},t)]\Delta t + F_i\Delta t \end{aligned} \quad (1)$$

where f_i is the probability of finding a particle at site $\vec{r}$ at time t, moving along the ith lattice direction defined by the discrete speeds $\vec{c}_i$ with $i = 1, ..., b$. The left hand-side of (2) stands for molecular free-streaming, whereas the right-hand side represents the time relaxation (due to collisions) towards local Maxwellian equilibrium. Finally, F_i represents the total volumetric body force. In particular, we shall use a *dynamic mean-field* term connected with bulk particle-particle interactions. The pseudo-potential force consists of two separate components $\vec{F}(\vec{r},t) = \vec{F}_1(\vec{r},t) + \vec{F}_2(\vec{r},t)$, defined as follows:

$$\begin{aligned} \vec{F}_1(\vec{r},t) &= G_1\psi(\vec{r};t)\sum_{i=0}^{b_1} w_i\psi(\vec{r}_{1i},t)\vec{c}_{1i}\Delta t \\ \vec{F}_2(\vec{r},t) &= G_2\psi(\vec{r};t)\sum_{i=0}^{b_1} p_{1i}\psi(\vec{r}_{1i},t)\vec{c}_{2i}\Delta t \\ &+ G_2\psi(\vec{r};t)\sum_{i=0}^{b_2} p_{2i}\psi(\vec{r}_{2i},t)\vec{c}_{2i}\Delta t \end{aligned} \quad (2)$$

In the above, the indices $k = 1, 2$ refer to the first and second Brillouin zones in the lattice (*belts*, for simplicity), and $\vec{c}_{ki}$, p_{ki} are the corresponding discrete speeds and associated weights (see Figure 1). Finally $\vec{r}_{ki} \equiv \vec{r} + \vec{c}_{ki}\Delta t$ are the displacements along the i-the direction in the k-th belt. Note that the second force $\vec{F}_2$ acts on both belts, so that the short (S) and mid-range (M) components of the force read as follows $\vec{F}_S(\vec{r},t) = \vec{F}_1(\vec{r},t) + \vec{F}_{21}(\vec{r},t)$, and $\vec{F}_M(\vec{r},t) = \vec{F}_{22}(\vec{r},t)$, where subscripts 21 and 22 indicate the component of $\vec{F}_2$ acting on the first and second belts respectively. Note that positive(negative) G correspond to repulsion(attraction) respectively and that G is a measure of potential to thermal energy ratio. The first belt is discretized with 9 speeds ($b_1 = 8$), while the second with 16 ($b_2 = 16$) and the weights are chosen in such a way as to fulfil the following relations [18]: $\sum_{i=0}^{b_1} w_i = \sum_{i=0}^{b_1} p_{i1} + \sum_{i=0}^{b_2} p_{i2} = 1$; $\sum_{i=0}^{b_1} w_i c_i^2 = \sum_{i=0}^{b_1} p_{i1}c_{i1}^2 + \sum_{i=0}^{b_2} p_{i1}c_{i2}^2 = c_s^2$, $c_s^2 = 1/3$ being the lattice sound speed. The numerical values of the weights are given in Table .

i	$\lvert c_i\rvert^2$	w_i	p_{i1}	p_{i2}
$1-4$	1	1/9	4/63	
$5-8$	2	1/36	4/135	
$9-12$	4			1/180
$13-20$	5			2/945
$21-24$	8			1/15120

Table 1: Links and weights of the two-belt, 24-speed lattice.

The pseudo-potential $\psi(\vec{r})$ is taken in the form first suggested by Shan and Chen [13], $\psi(\rho) = \sqrt{\rho_0}(1 - e^{-\rho/\rho_0})$ where ρ_0 marks the density value at which non ideal-effects come into play and it is fixed to $\rho_o = 1$ in lattice units. Taylor expansion of (2) to second-order delivers the following non-ideal equation of state (EOS) $p \equiv P/c_s^2 = \rho + \frac{(g_1+g_2)}{2}\psi^2(\vec{r},t)$, where $g_k \equiv G_k/c_s^2$ are normalised coupling strengths. Further expansion to fourth-order provides the following expressions for the surface tension

$$\gamma = -\frac{(G_1 + \xi G_2)}{2}c_s^4\int_{\infty}^{\infty}|\partial_y\psi|^2 dy \quad (3)$$

where y runs across the phase interface. Note that the double potential allows to change the equation of state and the surface tension independently. In particular, since $\xi = \mathbf{12/7} > \mathbf{1}$ the effect of the repulsive belt is to *lower* the surface tension at a given value of G_1+G_2. Thus, the mid-range potential is expected to act as a "surfactant" [1].

We have simulated droplet formation by integrating the LBE Eq. (2) in a 2D lattice using the nine-speed 2DQ9 model [12, 17], out of a noisy density background with initial density $\rho_{in} = \rho_0 ln2 + \delta\rho$ in a periodic domain. The force, however, is evaluated on a larger 24-speed stencil (see Fig. 1). In all simulations, $\tau = 1$ and $G_{eff} = G_1 + G_2 = -4.9$. This choice yields a surface tension $\gamma \approx 0.5$ and a density ratio $\frac{\Delta\rho}{\rho} \approx 10$ between liquid and vapour phases, respectively. In this configuration, we have studied the changes in the qualitative behaviour of the droplet formation as a function of the strength of the repulsive force. We have performed a systematic scan over the force strength, while keeping $G_{eff} = -4.9$ in the (G_1, G_2) plane, with a standard resolution of 128^2 grid points, and with final simulation time $t = 50000$. By defining a characteristic time-scale $t_{cap} = \frac{H\mu}{\gamma}$, μ being the dynamic viscosity of the fluid and H the dimension of the domain, the final time corresponds to about $50t_{cap}$. It has been checked that the the same qualitative behaviour is reproduced at higher resolution, 256^2 and 512^2 lattice sites. In analogy with droplet theory and kinetic Ising simulations [19, 20], we identify the following four regions: as follows; i) $|G_{eff}| \equiv |G_1 + G_2| < |G_c| = 4$: homogeneous

fluid (zero droplets); ii) $|G_{eff}| > |G_c|$, $G_2 = 0$: non-homogeneous fluid, one droplet (standard Shan-Chen); iii) $|G_{eff}| > |G_c|$, $0 < G_2 < G_{2c}$: non-homogeneous fluid (several metastable droplets); iv) $|G_{eff}| > |G_c|$, $G_2 > G_{2c}$: quasi-ordered fluid (many stable droplets, "emulsion");

An example of fluid behaviour in the metastable region iii) is given in Fig. 2, corresponding to $G_2 = 10$. From this figure, we observe that as many as 30 droplets are formed at time $t = 10000 \sim 10t_{cap}$, while at time $t = 30000$ and $t = 50000$, this number falls down to 11 and 7, respectively. A typical fluid configuration in the stable region iv) is given in Figure 3, corresponding to $G_2 = 13$ and $t = 50000$. From this figure, nucleation of quasi-ordered liquid droplets is apparent. It is interesting to observe that in this regime, the fourth order expression eq. (3) would yield an unphysical negative surface tension, indicating that higher order terms can no longer be neglected. Numerical exploration of this region shows however that the mesoscopic model continues to provide physically plausible results, with the surface tension smoothly decreasing by about a factor two with increasing G_2. This is consistent with the physical behaviour of surfactants, where the surface tension decreases by a factor of $2-3$ without ever vanishing [1].

The physical scenario is summarised in figure 4, where the interfacial area is plotted as a function of time. From this figure, we observe that the standard Shan-Chen fluid attains its single-droplet steady-state on a time scale of a few 'capillary' times, $5t_{cap} \sim 5000$ time-steps. Direct inspection (not displayed for space limitation) shows that the one-droplet configuration attains the lowest value of the pseudo-potential energy associated with the forces defined in eq. (2). By raising G_2, multi-droplet configurations are excited, as clearly displayed by the plateaux in the time evolution of the interfacial area $A(t)$ at different values of G_2. Each plateau associates with a given number of droplets, the transition between two different plateaux marking the discrete change in the number of droplets. From Figure 4 it is apparent that, even though in the limit $t \to \infty$ all configurations are expected to decay to the single-droplet ground state, the time it takes to reach this asymptotic state becomes increasingly larger as G_2 approaches the critical value G_{2c}. In fact, as $G_2 > G_{2c}$, this relaxation time is virtually infinite, corresponding to the attainment of a new stable phase, i.e. the quasi-ordered state represented in Figure 3. Remarkably, the present LB method permits to straddle across the entire region of metastability, connecting the one-droplet Shan-Chen state all the way to the quasi-ordered state. It is instructive to inspect the number of droplets at a given time as a function of the repulsive strength G_2. Such information is displayed in Figure 4b at times $t = 5, 10t_{cap}$ and $t = 50t_{cap}$. From this figure, we see that the number of droplets as a function of time is a monotonically non-decreasing function of G_2, with the smallest values of G_2 showing a clear tendency to relax to the same asymptotic value $n = 1$. This is consistent with the theoretical expectation of a single-droplet steady-state in the long-time limit in the region $G_2 < G_{2c}$.

Our numerical results are supported by the following theoretical considerations. In the single-droplet region, mass conservation delivers $\rho_l V_l + \rho_g V_g = \rho_i V = M$, where index i stands for initial conditions, $V_{l,g}$ denotes the total volume of the liquid/gas phase, and A is the interfacial area. The droplet radius, R, follows from a simple rearrangement: $\frac{\pi R^2}{H^2} = \frac{\rho_i - \rho_l}{\rho_l - \rho_g}$, where $\rho_{l,g}$ can be computed a priori by combining mechanical stability of the interface (zero divergence of momentum-flux tensor), with Maxwell's area rule [21], $\int_{\rho_l^{-1}}^{\rho_g^{-1}} (p(\rho) - p_0) d\rho = 0$, where p_0 is the constant bulk pressure. With our choice $G_{eff} = -4.9$, $\rho_i = \rho_0 ln2 = ln2$, we obtain $\rho_g \approx 0.17$ and $\rho_l \approx 1.85$, so that the liquid area covers approximately one third of the simulation box. This is confirmed by numerical experiments, which yield $\rho_g = 0.172$ and $\rho_l = 1.865$. The computed density predicts $R \approx 40$, in good agreement with the numerical value provided by the simulations. In our simulations, $R = 40$, Laplace's law $R = \frac{\gamma}{\Delta p}$ yields $\gamma = 0.0457$, in good match with the value $\gamma \approx 0.04$ obtained by numerically integrating the Eq.(3).

With two parameters at our disposal, G_1 and G_2, the present model allows a separate control of the equation of state and surface tension, respectively. In particular, the non-ideal part of the equation of state depends only on $A_1 = G_1 + G_2$, whereas surface tension effects are controlled by the combination $G_1 + \frac{12}{7} G_2$. Since in the vicinity of $\gamma \to 0$ higher order terms come into play, it proves expedient to define a new coefficient

$$A_2 = G_1 + \lambda G_2 \tag{4}$$

where the numerical factor λ plays the role of a renormalisation parameter, whose departure from zeroth-order value $\frac{12}{7}$ is a measure of the influence of the higher-order terms. We found that $\lambda \approx 3/2$ provides satisfactory agreement with the numerical results. Given this renormalisation, the numerical value of G_{2c} can be estimated by noting that, to fourth-order, the total force, $\vec{F_{tot}} = \vec{F_1} + \vec{F_2}$, in the present LB model is given by:

$$\vec{F_{tot}} = -\left(c_s^2 A_1 \psi \vec{\nabla} \psi + \frac{A_2 c_s^4}{2} \psi \vec{\nabla} \Delta \psi \right) . \tag{5}$$

A dimensional argument [1], gives $l^2 = \frac{c_s^2}{2} \frac{A_2}{A_1} = \frac{1}{6} \frac{A_2}{A_1}$, this yields

$$l \sim \frac{1}{\sqrt{6}} \sqrt{\frac{A_2}{A_1}} \;\rightarrow\; \frac{l}{l_1} = \sqrt{1 - \frac{G_2}{2|G_{eff}|}} \tag{6}$$

where l is the typical size of a nucleus and l_1 is the typical single-droplet dimension. The resulting spinodal value, at

[1] Strictly speaking, this estimate is only valid for droplets with radius significantly larger than the lattice spacing, $\Delta x / l \ll 1$.

which $l \to 0$, turns out to be $G_{2c} = 9.8$. For this value, the second term in Eq. (5) diverges, thus signaling a phase transition. This value is found to be in good agreement with the numerical simulations, which indicate complete nucleation starting around a value of $G_2 \approx 10$, as shown in fig. 4.

The spinodal point can also be estimated by resorting to classical homogeneous nucleation theory [22]. On the basis of this theory, the equilibrium cluster distribution for a cluster of size n is given by:

$$p_e(n) = p_e(1) \exp\left[-\frac{2\pi R(\gamma_n\sqrt{n} - \gamma_1)}{KT}\right] \qquad (7)$$

where $\gamma_n < \gamma_1$ is the value of the surface tension such that the equilibrium distribution would correspond to a n-droplet configuration. The expression (7) builds on two assumptions: i) the equilibrium cluster distribution has the form $p_e(n) \sim \exp[-W(n)/KT]$ and ii) $W(n)$ is equal to the product of the area of the cluster and the surface tension of a flat liquid surface with the same temperature and composition of the nucleus and (i.e. $W(n) = \gamma A(n)$). Moreover, the volume of a droplet is given by πR^2, while with n droplets, the same volume is $\pi n R_n^2$, so that $R_n \approx R/\sqrt{n}$. Finally, all nuclei are assumed to be spherical and with the same radius. Based on the expression (7), the surface tension $\gamma = \gamma_1/\sqrt{n}$ would vanish in the limit $n \to \infty$, corresponding to $l \to 0$. By inspecting the expression (3), and taking into account the definition of G_{eff}, $\gamma = 0$ implies $G_{2c} = 2|G_{eff}|$, consistently with the expression (6). Let us define $G_2(n)$ as the value of G_2 such that the n-droplet configuration is allowed to survive the longest before decaying into the $n = 1$ ground state, i.e. $G_1 + \frac{3}{2}G_n = 1/\sqrt{n}$. By recalling that, by definition, $G_1 + \frac{3}{2}G_{2c} = 0$, the following scaling relation is readily obtained: $n = (1-\xi)^{-2}$, where we have set $\xi \equiv G_2/G_{2c}$. Interestingly, a dynamic extension of such scaling law, namely $n(t) = (1-\xi)^{-p(t)}$ provides a reasonable fit of the numerical data, with $p(t) \sim 2$ at small t, and $p(t) \to \infty$ (step-function) at $t \to \infty$.
Larger simulations (512^2) confirm the basic picture described in this paper, namely a seamless transition from a homogeneous gas to a quasi-ordered configuration of droplets, whose size (number) is controlled by the relative strength of repulsive and attractive interactions. As an example, in Figure 5 the spectrum of density fluctuations is shown in the initial and final stage of the evolution. The typical size of the droplets is identified with the inverse wave-number $2\pi/k_{max}$, where k_{max} is the wave-number at which the peak of the spectrum is attained ($k = 1$ corresponds to a droplet radius $R = L$). From this figure we see that with $G_1 = -15$ and $G_2 = 10.1$, the peak is around $k \sim 4$, while the SC case gives $k \sim 1$, corresponding to about 16 droplets in the same volume.

Summarising, we have shown that the inclusion of a mid-range repulsive potential within the Shan-Chen formulation of non-ideal lattice fluids, discloses a very rich physical picture. In particular, it opens up the possibility

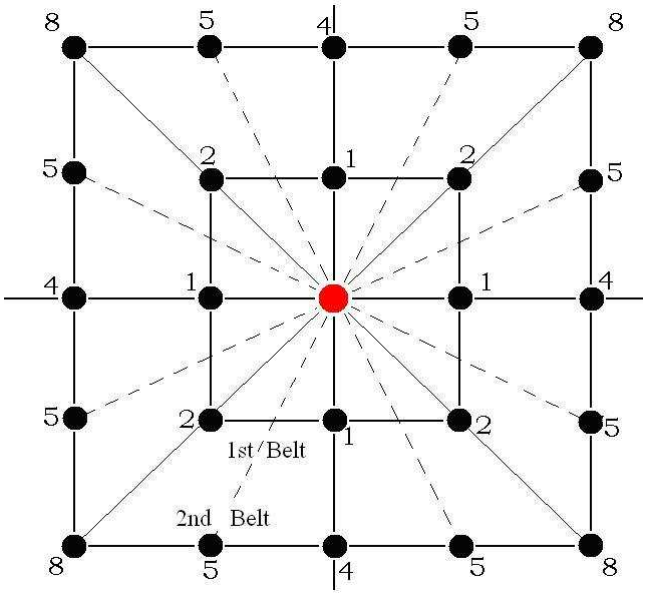

Fig. 1: Sketch of the discrete-velocity stencil used in the extended Lattice Boltzmann scheme. The integers denote the magnitude of the corresponding discrete speed.

of realising multiphase flows with long-lived metastable states characterised by multi-droplet configurations. The model allows the independent tuning of the size of the droplet and of the density ratio between the liquid and the gas phases. This should permit the efficient handling of complex applications, such as micro-emulsions [23], multiphase sprays, globular protein crystallisation [24] and, possibly, glassy-like states as well.

SS wishes to acknowledge financial support from the project INFLUS (NMP3-CT-2006-031980) and SC from the PI2S2 COMETA project also supported by a Marie-Curie UE grant. Fruitful discussions with M. Sbragaglia, R. Benzi, L. Biferale, I. Procaccia and F. Toschi are kindly acknowledged.

REFERENCES

[1] P.G. de Gennes, *Capillarity and wetting Phenomena* (Springer, New York, 2003).
[2] J.S. Rowlinson and B. Widom, *Molecular Theory of Capillarity* (Clarendon, Oxford, 1982).
[3] M. Seul and D. Andelman, *Science* 267, 476 (1995).
[4] B.P. Stojkovic et al., Phys. Rev. Lett., **82**, 4679, (1999).
[5] C. Reichhardt, C.J. Olson Reichhardt, I. Martin, and A.R. Bishop, Phys. Rev. Lett., **90**, 026401, (2003).
[6] E. Tuzel, G. Pan, T. Ihle, D.M. Kroll, Europhys. Lett., **80**, 40010, (2007).
[7] R. Clift, J. R. Grace, and M. E. Weber, *Bubbles, Drops and Particles*, (Academic Press. New York, 1978)

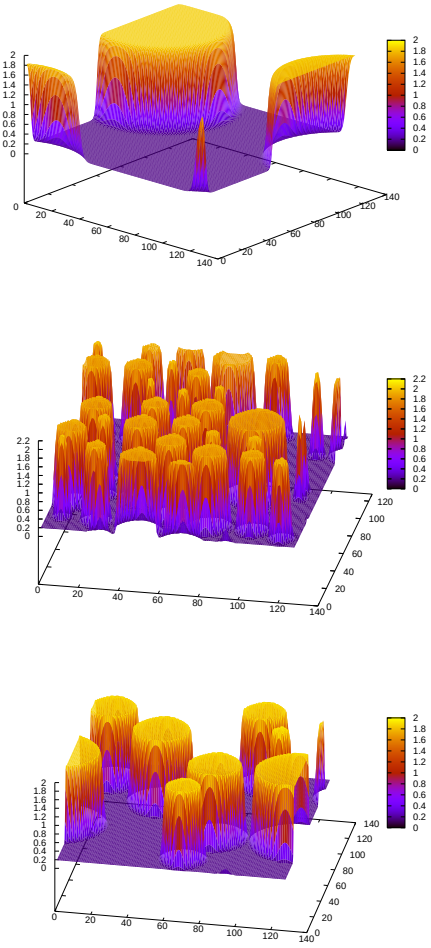

Fig. 2: Spatial distribution of the fluid density. The formation of a large number of droplets is well visible. Configuration parameters: $G_{eff}/G_c = -4.9$, $nx = ny = 128$; 2a: Single droplet (standard Shan-Chen), $t = 50t_{cap}$, 2b: Multi-droplet, $G_2 = 10$, $t = 10t_{cap}$. 2c: Multi-droplet, $G_2 = 10$, $t = 50t_{cap}$.

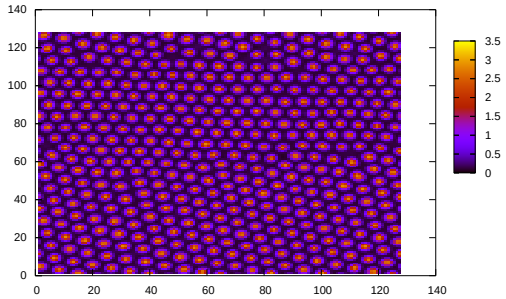

Fig. 3: Isocontours of the density distribution at time $t = 10000 \sim 10t_{cap}$, $G_{eff}/G_c = -4.9$, $nx = ny = 128$, $\mathbf{G_2 = 19}$. The configuration contains approximately 100 droplets. Note that the droplet radius is about $128/15/2 \sim 4$ lattice units, still sufficiently larger than the lattice thermal length $\Delta t c_s \sim 1/\sqrt{3}$. This is usually sufficient to rule out serious non-hydrodynamic effects, although this issue is surely worth a detailed future investigation.

[8] G. R. Mc Namara, G. Zanetti, Phys. Rev. Lett., **61**, 2332, (1988).

[9] F. Higuera, S. Succi, R. Benzi, Europhys. Lett., **9**, 345, (1989)

[10] S. Ansumali, and Iliya V. Karlin Phys. Rev. Lett. **95**, 260605 (2005).

[11] R. Benzi, S. Succi, M. Vergassola, Phys. Rep., **222**, 145, (1992).

[12] S. Chen , and G.D. Doolen, Annual Rev. Fluid Mech., **30**, 329 (1998).

[13] X. Shan, and H. Chen Phys Rev E **47**, 1815 (1993).

[14] Falcucci G., Bella G., Chiatti , Chibbaro S., Sbragaglia M., and Succi S., Communications in Computational Physics, Vol. 2, No. 6, pp. 1071-1084.

[15] J.P. Boon, C. Bodenstein, D. Hanon J. Mod. Phys. C **9**, 1559 (1998).

[16] S. Succi *Lattice Boltzmann equation for Fluid Dynamics and beyond* (Oxford U.P. 2001).

[17] D.A. Wolf-Gladrow *Lattice-gas Cellular Automata and Lattice Boltzmann Models* (Springer, Berlin, 2000).

[18] M. Sbragaglia, R. Benzi, L. Biferale, S. Succi, K. Sugiyama, and F. Toschi, Phys. Rev. E **75**, 026702 (2007).

[19] P. A. Rikvold, H. Tomita, S. Miyashita, and Scott W Sides, Phys. Rev. E **49**, 5080, (1994).

[20] V.I. Kalikmanov , *Statistical Physics of fluids* (Springer, Berlin, 2001).

[21] R. Benzi, L. Biferale, M. Sbragaglia, S. Succi, and F. Toschi, Phys. Rev. E **74**, 021509 (2006).

[22] J. L. Katz, Pure & Appl. Chem. **64**, 1661 (1992).

[23] M. Nekovee, P. V. Coveney, H. Chen, and B.M. Boghosian Phys. Rev. E **62**, 8282, (2000).

[24] S. Brandon, P. Katsonis, and P.G. Vekilov, Phys. Rev. E **73**, 061917, (2006).

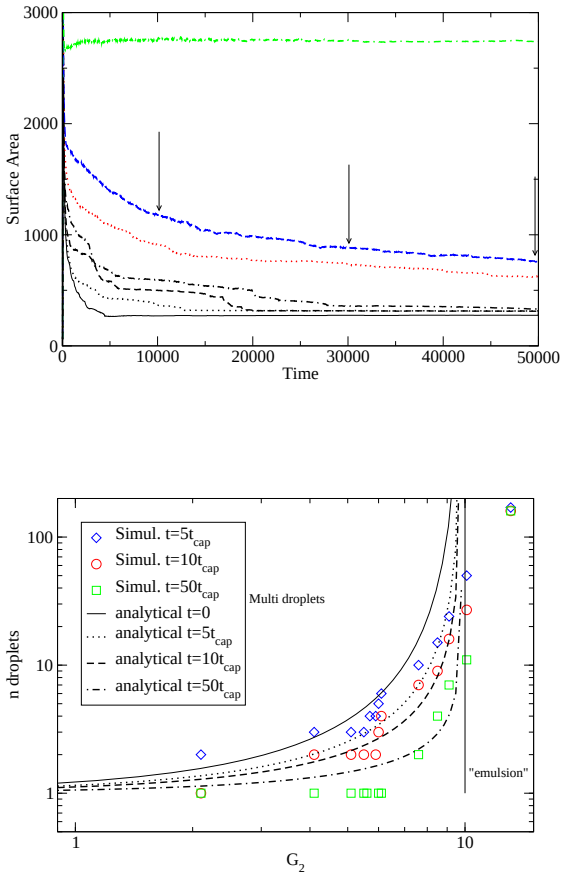

Fig. 4: Fig 4a: Total interfacial area (perimeter in 2D) as a function of time at increasing values of $G_2 = 0, 4.1, 6.1, 7.6, 9.1, 10, 13$. The final time, $t = 50000$ time-steps, corresponds to $50t_{cap}$. The arrows indicate times at which density snapshots are shown in the previous figures. Fig 4b: Number of droplets versus G_2 at $t = 5, 10, 50t_{cap}$. The vertical line denotes the theoretical spinodal point G_{2c}. The single-droplet region is associated with $G_2 \to 0$. The analytical fit $n(t) = (1-\xi)^{-p(t)}$, with $p(t) = \frac{2}{1+t/10}$, is also shown.

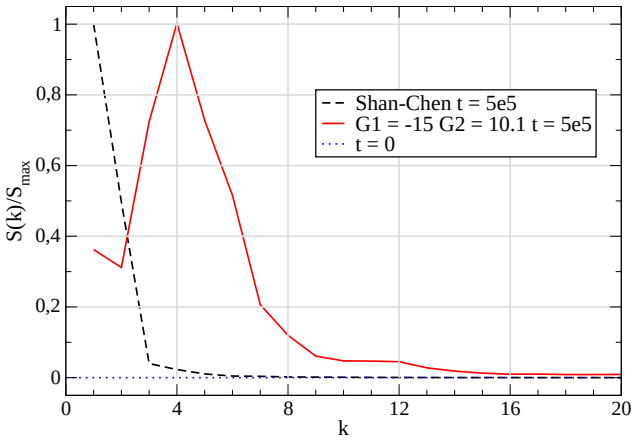

Fig. 5: Spectrum of density fluctuations, normalized to its peak value, for the standard Shan-Chen (dashed) and for the case $G_1 = -15$ and $G_2 = 10.1$ (solid line) after 5×10^5 time-steps. The latter case shows a clear shift in the spectrum, peaked around $k = 4$. This indicates a reduction of about a factor 4 in droplet size, corresponding to approximately 16 droplets in the computational box. The dotted line corresponds to spectrum at $t = 0$, with fluctuations of the order of 10^{-5}, not visible on the scale of the figure. Grid size 512^2.